Journal of Applied Physics

RESEARCH ARTICLE | MARCH 09 2026

Current shunting and plasma instabilities during electrical explosions of copper and aluminum wires in water and air

R. Grikshtas ✉ ; N. Asmedianov ; S. Pavlov ; I. Yungerman ; A. Rososhek ; J. Strucka ; K. Mughal ; B. Lukic; M. Liverts ; T. White ; R. Bean ; J. Bielecki ; R. Letrun ; T. Popelar; E. Sobolev ; F. Trost; J. C. P. Koliyadu ; T. Sato ; P. Vagovic ; S. N. Bland ; Ya. E. Krasik

J. Appl. Phys. 139, 103301 (2026)
https://doi.org/10.1063/5.0320019

Journal of Applied Physics ARTICLE pubs.aip.org/aip/jap

Current shunting and plasma instabilities during electrical explosions of copper and aluminum wires in water and air

Cite as: J. Appl. Phys. **139**, 103301 (2026); doi: 10.1063/5.0320019
Submitted: 28 December 2025 · Accepted: 18 February 2026 ·
Published Online: 9 March 2026

R. Grikshtas,[1,a)] N. Asmedianov,[1] S. Pavlov,[1] I. Yungerman,[1] A. Rososhek,[1] J. Strucka,[2,3] K. Mughal,[2] B. Lukic,[4] M. Liverts,[5] T. White,[6] R. Bean,[3] J. Bielecki,[3] R. Letrun,[3] T. Popelar,[3] E. Sobolev,[3] F. Trost,[3] J. C. P. Koliyadu,[3] T. Sato,[3] P. Vagovic,[3,7] S. N. Bland,[2] and Ya. E. Krasik[1]

AFFILIATIONS

[1]Physics Department, Technion—Israeli Institute of Technology, Haifa 3200003, Israel
[2]Plasma Physics Group, Imperial College London, London SW7 2BW, United Kingdom
[3]European XFEL GmbH, Holzkoppel 4, Schenefeld 22869, Germany
[4]European Synchrotron Radiation Facility, CS40220, Grenoble Cedex 9 380043, France
[5]FLOW, Department of Engineering Mechanics, KTH Royal Institute of Technology, Stockholm 100 44, Sweden
[6]Department of Physics, University of Nevada, Reno, Nevada 89557, USA
[7]Center for Free-Electron Laser Science CFEL, Deutsches Elektronen-Synchrotron DESY, Notkestr. 85, Hamburg 22607, Germany

[a)]**Author to whom correspondence should be addressed:** ron.gri@campus.technion.ac.il

ABSTRACT

We present the first x-ray images of electrically exploding wires in air and water, captured at the European X-ray Free-Electron Laser (EuXFEL). These images reveal current shunting in a copper wire during its explosion in air, and the development of electrothermal (and possibly magnetohydrodynamic) instabilities in copper and aluminum wires exploding in water. The experiments were conducted at the Single Particles, Clusters, and Biomolecules and Serial Femtosecond Crystallography instrument (SPB/SFX) at EuXFEL, where fine metallic wires were driven by a pulsed-power generator with a current rise time of ∼1.1 μs and a peak amplitude of ∼28 kA. EuXFEL enabled MHz x-ray radiography of the wires using 20 keV photons and a narrow bandwidth of ∼40 eV. Using the specific current action integral for a copper wire explosion, we provide the first quantitative estimate of the fraction of current that is shunted through the surrounding medium of an exploding wire. Fourier analysis of the electrothermal instability spectrum shows that its wavelength remains mostly independent of the wire diameter once it has exploded, and that the temperature perturbation is similar in magnitude to the average temperature in the wire.

I. INTRODUCTION

Warm Dense Matter (WDM) represents the crossover between the condensed phase and the plasma state, in which strong ion coupling in the plasma significantly alters its expected properties. WDM is characterized by temperatures of several eV, pressures of several gigapascals, and near-solid densities, making it central to high-energy density physics and inertial confinement fusion.[1,2] One effective experimental method for producing and investigating WDM is through electrical wire explosions (EWE),[3–6] wherein high current densities ($\geq 10^7$ A/cm^2) generate rapid Ohmic heating accompanied by phase transitions and plasma formation.[7] Indeed, exploding wires are the basis for many conductivity models and equations of state in the warm, dense regime,[8–10] and understanding the behavior of such exploding wires is key to simulating wire array Z-pinches,[11] soft x-ray sources,[12,13] and nano powders production.[14]

When a wire explodes in air or vacuum, an unknown fraction of the current ceases to remain confined within the wire and is instead diverted into the surrounding medium.[15–17] This process,

known as current shunting, limits the energy deposited into the wire.[18] The accepted mechanism for this shunting involves the rapid impact ionization of the ambient gas near the heated wire surface by thermionic emitted electrons. This leads to avalanche flashover and the formation of a plasma sheath along the wire, which provides a parallel current path that bypasses the wire core.[7] In Refs. 19 and 20, electrical explosions of wires made of various materials in air and vacuum were investigated. Using electrical, optical, laser shadowgraphy, and Schlieren diagnostics, the authors proposed two possible scenarios for the formation of high-conductivity, current-carrying plasma channels. One scenario assumes that the wire remains in a low-conductivity state, leading to plasma formation along the wire surface due to ionization of desorbed gases or surrounding air molecules. This plasma captures part of the current, thereby reducing the energy density deposited into the wire. The second scenario suggests that the wire conductivity is sufficiently high to prevent the formation of surface plasma; instead, a high-conductivity plasma forms due to avalanching within the wire material, and the entire energy is deposited into the wire. However, despite extensive studies of EWE in gases and vacuum, no quantitative estimates of the current flowing through such surface plasma channels have been reported, owing to the inherent difficulty of separating this contribution from the total discharge current. Conversely, in underwater environments, this surface breakdown is suppressed by the high density and dielectric strength of water,[21] thereby preventing the formation of such a shunting plasma channel.[22,23] In addition, the low compressibility of water suppresses rapid wire expansion, thereby allowing a higher energy density deposition to be maintained.[24] Indeed, at pressures of $\lesssim 5 \times 10^9$ Pa, values realizable in the vicinity of an exploding wire, the isothermal Tait–Murnaghan equation of state[25] yields a water compression of $\delta = \rho/\rho_0 \leq 1.47$.

All types of wire explosions (in vacuum, air, or water) are subject to the electrothermal instability (ETI), which has received growing attention over the last few decades.[26] Small imperfections within the material, such as micrometer-scale grains or voids, can initiate this instability.[27] Due to the decrease in conductivity with temperature, this leads to radial re-distribution of the current density and formation of a hot layer in the axial direction. The latter compresses adjacent outer layers, slightly increasing their conductivity. Thus, one obtains adjacent layers with lower temperatures, higher densities, and lower resistivities. This process results in the formation of a striated pattern of layers along the axial direction of the wire, with density and temperature modulations exhibiting a characteristic minimal wavelength. It should be noted that in the case of a (near) ideal plasma, where the resistivity decreases with temperature, the striations form parallel to the current direction.[28] Later in time, providing the current remains high enough, instabilities driven by current density—"magnetohydrodynamic (MHD) instabilities" may come to dominate a wire explosion. One of the most significant ones in EWE is the $m = 0$ ("sausage") instability,[29,30] which becomes pronounced when its typical development time $\tau_{\text{inst}} = r_0/V_A$, determined by the wire radius r_0 and the Alfven velocity V_A, becomes smaller than the wire explosion time. The latter is determined by the specific current action integral for the wire material and the time-dependent current density.[31]

Until recently, analyzing fine-scale instabilities in exploding wires, particularly in the dense, optically thick plasma of an underwater explosion, was challenging. However, new diagnostic capabilities with high-speed x-ray imaging have made it possible to directly observe these phenomena. Synchrotron x-ray radiography, in particular, has proven effective for capturing the internal structure of exploding wires with high spatial and temporal resolution.[32,33] This method was previously used to initially identify ETI in underwater electrical wire explosions (UEWEs) of copper,[34] to investigate jet formation in wire arrays,[35] and, more recently, to analyze the minimal ETI wavelength across various materials.[36]

In this article, we present the first use of multi-frame quasi-monochromatic (~40 eV bandwidth) MHz x-ray radiography on an X-ray Free-Electron Laser source (XFEL)[37] to image electrical explosions of copper wires in air and underwater electrical wire explosions (UEWEs) of copper and aluminum wires. The main advantages of this source are its narrow bandwidth, which allows for better estimates of the densities produced as a wire explodes, and the ultra-short (30 fs) exposures that can be used in very rapidly evolving situation experiments. The wires were exploded using a microsecond (μs) timescale pulse generator, and their expansion was imaged by the Single Particles, Clusters, and Biomolecules and Serial Femtosecond Crystallography (SPB/SFX) instrument at European X-ray Free-Electron Laser (EuXFEL) in Schenefeld Germany. Our results show that wire expansion in air occurs later than in water due to plasma current shunting along the wire surface. This allows us to provide, for the first time, an estimate of the shunted current fraction derived from the specific action integral. Additionally, both ETI and larger-scale instabilities were resolved by MHz x-ray radiography during the explosion process. ETI was demonstrated not to evolve significantly over time and showed little variation between copper wires of different diameters. Using the measured x-ray transmission through the wire, we estimated that at the time of observation, specifically at $t \geq 1.04\,\mu$s when the wire transfers to vapor-low ionized plasma state, both the density and temperature of the wire vary on a scale comparable to their mean values, indicating that the linear ETI model might be invalid for underwater wire explosions. Lastly, we report a pronounced hydrodynamical instability in aluminum wires, which could be related to local inhomogeneities in the aluminum wire or its oxide coating, leading to earlier explosion at that location.

II. EXPERIMENTAL SETUP AND DIAGNOSTIC METHODS

Experiments were carried out using a μs-timescale pulsed-power driver, previously used in synchrotron facilities.[32,33] The generator consists of four low-inductance high-voltage (HV) Maxwell capacitors, 220 nF each, connected in parallel and discharged by a triggered spark-gap switch. When charged to a 28 kV (total stored energy of 345 J), the generator delivers a maximal current amplitude of ~28 kA within a rise time of ~1.1 μs.

Diagrams of the experimental setup, generator chamber, and tested capsules are shown in Fig. 1. Single wires made of copper (Cu) and aluminum (Al), each 35 mm long with different diameters (0.16, 0.20, and 0.25 mm for Cu; 0.25 mm for Al), were stretched inside a polymethyl methacrylate (PMMA) capsule [inner/outer diameter of 4/8 mm, respectively, see Fig. 1(a)] filled

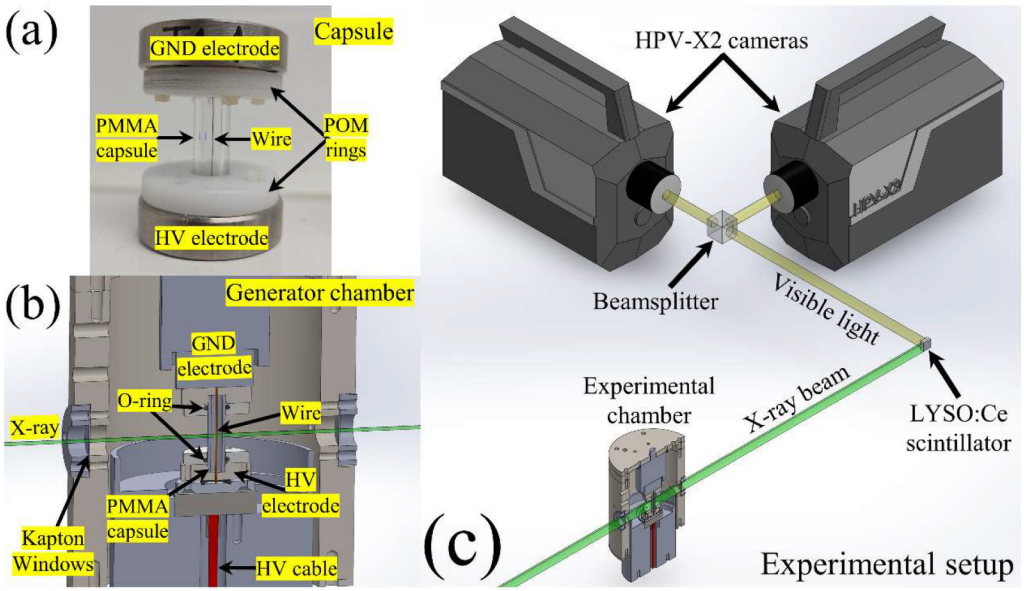

FIG. 1. Illustration of a capsule with a wire stretched between the electrodes (a); experimental system close up of the generator chamber (b) and optical setup (c).

with de-ionized water. Two polyoxymethylene (POM) rings secured the PMMA capsule and pressed against a set of rubber O-rings to prevent leaks. This capsule was placed on a high-voltage (HV) electrode [see Fig. 1(b)] inside the generator experimental chamber, with the HV electrode connected to the pulse generator using a 50 cm length cable. Current (I) and voltage (V) waveforms were measured with a self-integrated Rogowski coil (measurement error of ±3%) and a P6015 A Tektronix voltage divider (measurement error of ±5%), respectively. Waveforms were recorded using a Tektronix DPO4104 oscilloscope (1 GHz, 5 Gs/s), and the resistive voltage was calculated by subtracting the inductive voltage from the measured voltage as $V_r = V - L\frac{dI}{dt}$, where L is the self-inductance of the load within ±10% error. The contribution of the changing inductance IdL/dt is assumed to be negligible in the calculation of V_r.

The MHz x-ray radiography during the explosion was captured using the SPB/SFX instrument at EuXFEL, providing a 30 fs pulse with a photon energy of 20 keV (~40 eV energy bandwidth) at a repetition rate of 2.25 MHz (443 ns between pulses, ~300 μJ energy per pulse).[37] The x-ray beam, with a diameter of 1.3 mm, propagated through the experimental chamber which had two dielectric (Kapton) windows [Fig. 1(c)]. After illuminating the sample, the beam traveled ~0.6 m downstream, where it was converted into visible optical light by a 150 μm LYSO:Ce scintillator. This light was directed via a beam splitter to a pair of ultrahigh-speed framing Shimadzu corp. cameras (Japan, type HPV-X2) that operated at an alternating sequence with a frequency synchronized with the x-ray pulses. Each camera's total image size was 1.2 mm wide by 0.8 mm high.

To supplement experiments, one-dimensional MHD (1D MHD) simulations, described in Refs. 38 and 39, have been used for copper wire explosions. These simulations solve the hydrodynamic equations in Lagrangian mass coordinates, along with Maxwell's equations and Ohm's law on a two-region grid of metal and surrounding water. These equations are coupled with SESAME equations of state[40] and semi-empirical conductivity models,[38,41] where the fitting parameters are the conductivity at the critical point σ_{cr}[7] and the dependence of conductivity on temperature in the solid phase α.[41] The experimental ETI wavelength was determined through Fourier analysis as described in Ref. 36, and the uncertainty in the measured wavelength is estimated at ±10 μm due to edge smearing of the ETI and the unbiased standard deviation.

III. EXPERIMENTAL RESULTS AND DISCUSSION

A. Using underwater EWE of Cu wires to estimate current shunting in air explosions through the specific action integral

First, we present in Figs. 2(a) and 2(b) the waveforms of current, resistive voltage, resistance, and deposited power and energy obtained in an experiment with a 0.20 mm diameter Cu wire explosion in water. The explosion initiates at ~0.92 μs with a current amplitude of ~22 kA, a radius of 0.18 mm, and an average current density of ~2.2×10^7 A/cm^2. At around ~1.17 μs, corresponding to the Full Width at Half Maximum (FWHM) of the power, the energy deposited into the wire was ~52% of the generator's stored energy, with an energy density near 18 kJ/g at an energy deposition rate of ~4.6×10^{10} J/(g s). These finding are consistent with those presented in Ref. 34, which used the same generator and similar wire diameter. The resistance of the wire reaches ~2.2 Ω, indicating the formation of a low ionized high-resistivity

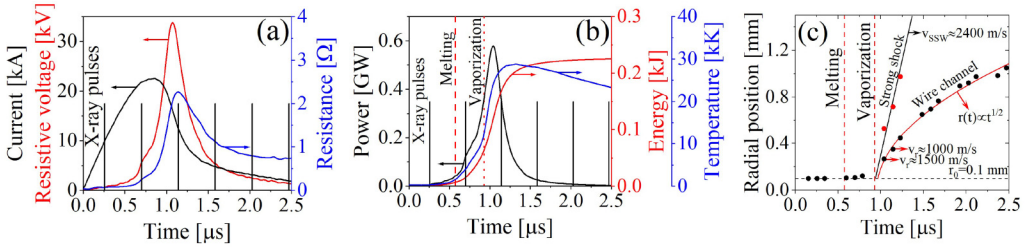

FIG. 2. Waveforms of (a) current (black), resistive voltage (red), and time-dependent resistance (blue), (b) deposited power (black), energy (red), and simulated temperature (blue) and trajectories of strong shock (red) and wire expansion (black) obtained from radiography images (c) obtained in underwater electrical explosions of 0.20 mm diameter and 35 mm length Cu wire. The timing of x-ray pulses train is marked with vertical black lines in (a), and the thermodynamical transitions are noted in (b) using dashed and dotted lines.

plasma. 1D MHD simulations show that maximum temperature reaches ~2.5 eV, placing the wire in the "warm dense matter" regime with coupling parameter $\Gamma > 1$.[2] In Fig. 2(c), we present the radial position of the strong shock front and the trajectories of the expanding wire, measured from radiography images with shifted timings and fitted to a Taylor–Sedov cylindrical blast wave model[42] (see examples in Fig. 3). It is evident that the onset of shockwave generation closely coincides with the start of rapid wire expansion and the moment when the deposited energy becomes sufficient to fully vaporize the wire. These data enable the estimation of the shock velocity at 2400 ± 50 m/s and the average wire expansion velocity during 1040–1140 ns at ~1000 m/s. Extrapolating the shock and wire expansion trajectories back to the initial radius of the wire, r_0, yields an onset time near ~950 ns. This occurs shortly after the energy needed for complete vaporization has been deposited and when the discharge current begins to decline. This is consistent with our definition of the wire explosion, which is characterized by the transition of the wire into a vapor—highly resistive plasma state, and when its internal pressure exceeds the self-magnetic field pressure.

A sequence of x-ray radiographic images showing an exploding 0.20 mm diameter Cu wire in water is presented in Figs. 3(a)–3(h), where time t is measured relative to the start of the current. At $t = 0.7\,\mu$s [Fig. 3(c)], the wire has expanded to a radius of 0.105 mm, ~0.2 μs after sufficient energy was deposited for melting. This agrees satisfactorily with estimates of volumetric thermal expansion, which for copper can be taken to be 3 μm at the wire's melting temperature.[43] At $t = 1.14\,\mu$s [Fig. 3(d)], when the wire transitions to low ionized high-resistivity plasma [see Fig. 2(a)], one can already observe well-developed ETI as alternating density layers and a strong shockwave propagating from the exploding wire. Later, at $t = 2.03\,\mu$s, when the current decreases to <3 kA, the contrast between adjacent layers diminishes (i.e., becomes "smeared"), indicating damping of density perturbations [see Fig. 3(f)].

Results of 1D MHD simulations of exploded Cu wires with diameters of 0.16, 0.20, and 0.25 mm are detailed in Fig. 4. These include the radial distributions of pressure [(a), (d), and (g)], density [(b), (e), and (h)], and temperature [(c), (f), and (i)] in the wires and surrounding water at 1, 2, and 3 μs after the current

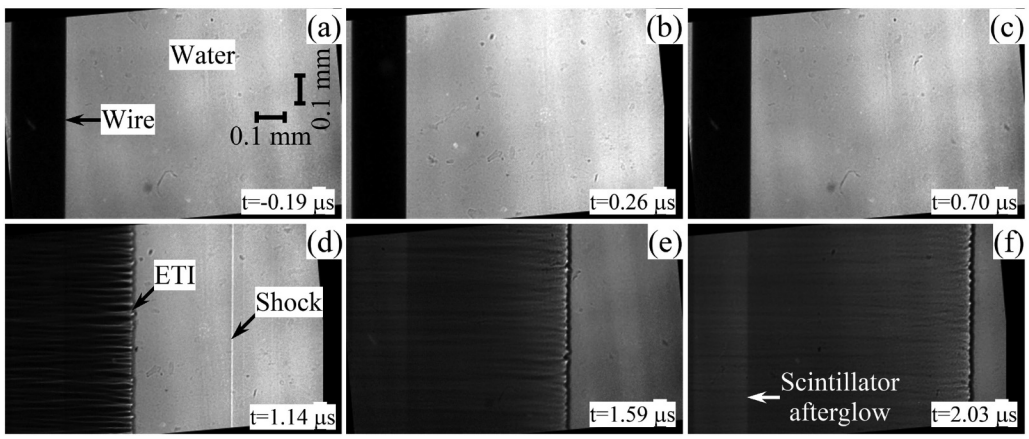

FIG. 3. Shadow x-ray radiography images with subtracted background of exploding 0.20 mm diameter Cu wire. All times are given relative to the start of the current discharge, and the ruler in (a) applies to all frames.

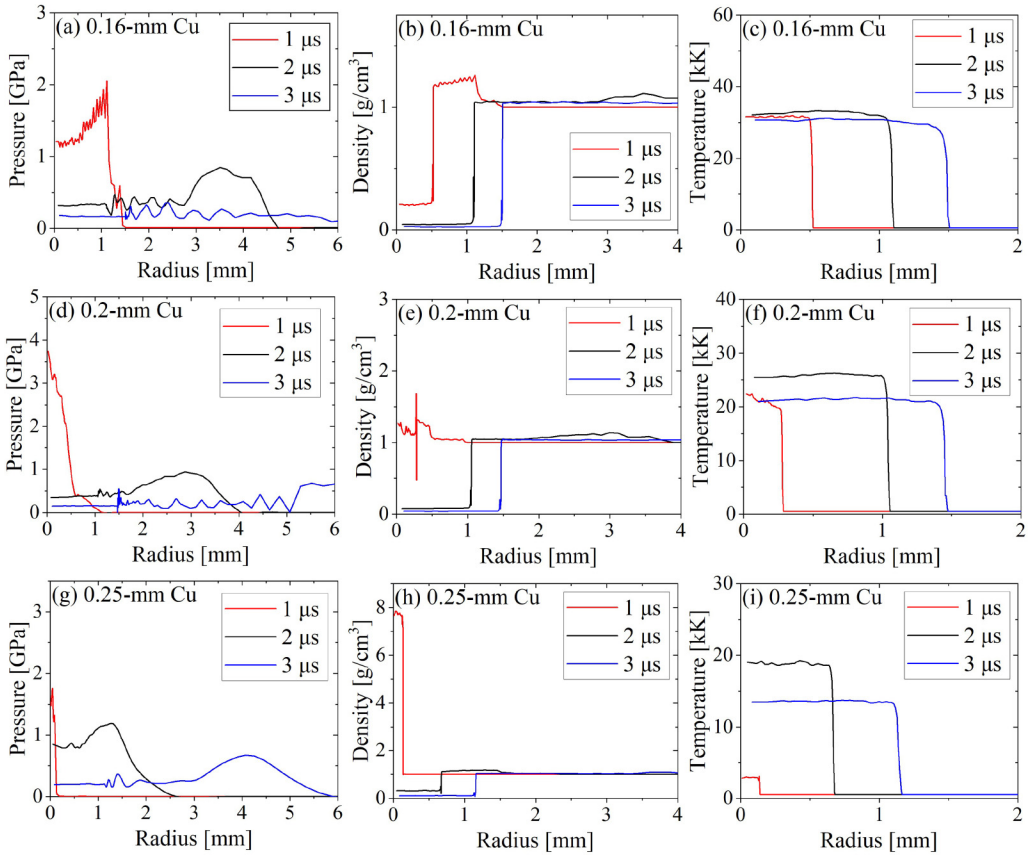

FIG. 4. Plots of simulated pressure, density, and temperature of the explosion of copper wires with diameters of 0.16 mm [(a)–(c)], 0.20 mm [(d)–(f)], and 0.25 mm [(g)–(i)] at various times after the discharge current onset (red—1 μs, black—2 μs, and blue—3 μs).

begins. These results were obtained by adjusting σ_{cr} and α values to match the current and voltage waveforms. One can observe the propagation of the strong shocks in water [Figs. 4(a), 4(d), and 4(g)], propagating at ~2500 m/s, and the channel expansion traveling at ~700 m/s, both consistent with the experimental data. The wire temperature generally remains uniform at 2–3 eV across the radius [Figs. 4(c), 4(f), and 4(i)], with thinner wires exhibiting higher overall temperatures and continuous heating caused by early explosion and underdamped discharge. The high density of the 0.25 mm wire [Fig. 4(h)] at 1 μs compared to the other wires [Figs. 4(b) and 4(e)] suggests that the wire did not explode at this point. It is understood that these 1D MHD simulations cannot replicate the development of ETI instability observed in experiments.

In contrast to wire explosions in water, Figs. 5 and 6 show the waveforms and x-ray radiography of the same diameter Cu wire explosion in air. In this experiment, the generator was charged to only 25 kV, which resulted in slightly slower current amplitude. However, it is clear that, although the current begins to decay at ~0.9 μs, not enough energy is deposited to vaporize the entire wire, as confirmed by radiography images [Fig. 6(d)]. Here, the wire has only expanded to $r = 0.115$ mm at $t = 1.1\,\mu$s. In comparison, for UEWE at nearly the same time, despite the water background, the wire has already expanded to $r = 0.35$ mm [see Fig. 3(d)]. Full vaporization energy is only achieved at ~1.33 μs, assuming full energy deposition into the material. The next x-ray image $t = 1.55\,\mu$s [Fig. 6(e)] shows significant wire expansion with visible ETI, and by $t = 1.99\,\mu$s [Fig. 6(f)], the wire has expanded beyond the frame borders. This suggests an expansion velocity of at least ≥1500 m/s, which is considerably faster than in water (≤1000 m/s), likely because water's density significantly dampens the explosion.

For the air explosion, the low energy density of ~10.7 kJ/g, half the energy density deposition rate of $\sim 1.9 \times 10^{10}$ J/(g s) compared to an underwater explosion and the late expansion suggest that a significant fraction of the current flows outside of the wire due to the formation of the shunting plasma.[7] Considering the expansion velocity of the wire and expansion of its radius [see Fig. 6(e)], the moment of explosion, when the wire starts to expand at a velocity of ~1500 m/s, can be estimated at $t \approx 1.4 \pm 0.1\,\mu$s.

To determine the fraction of current shunted by the surface plasma of the wire, we use of the specific current action integral h, which defines the energy deposition needed to achieve an explosion

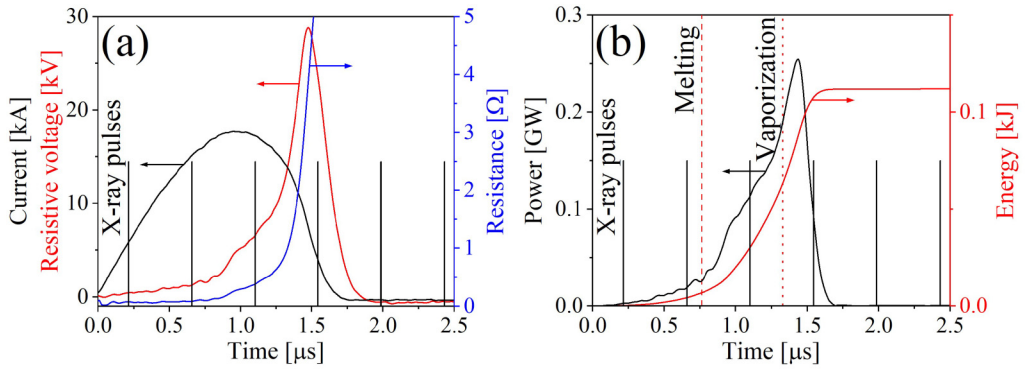

FIG. 5. Same as Fig. 2 but for a 0.20 mm Cu wire explosion in air (excluding the simulated temperature).

in EWE,[44,45]

$$h = \int_0^{t_{exp}} j^2 dt, \tag{1}$$

where $j(t) = I(t)/\pi r^2(t)$ is the current density, integrated from the start of the current $t = 0$ to the moment of explosion t_{exp}. In the case of the 0.20 mm diameter Cu wire explosion in water (see Fig. 2), at $t = 1.1\,\mu s$ relative to the beginning of the discharge current when approximately maximal power is deposited, the wire has expanded from an initial radius of $r_0 = 0.1$ mm to $r = 0.35$ mm. This occurs despite the resistance of water due to internal pressure exceeding the magnetic pressure produced by the discharge current. The specific action integral was calculated to be $h_{water} = 1.7 \pm 0.2\ A^2 \cdot s/cm^4$ at $t = 0.9\,\mu s$ when the current reaches its maximum value, based on the measured current, observable wire expansion from radiography, and the absence of shunting current.[18,39]

However, for a similar wire explosion in air at $t = 1.1\,\mu s$, the wire has only expanded to $r = 0.115$ mm which is significantly smaller than for underwater wire explosions. This can occur only if part of the current flows not through the wire, but through a plasma formed along the wire surface. Since the total current remains the same, the magnetic pressure surrounding the plasma channel and the exploding wire is identical for air and underwater explosions. Therefore, the reduced wire expansion observed in air indicates that the current flowing through the surrounding plasma channel does not contribute to wire heating or to the buildup of internal pressure. At $t = 0.94\,\mu s$, we calculate the value $h_{air} = 1.3 \pm 0.1\ A^2\,s/cm^4$, assuming insignificant wire expansion. Under the assumption that explosions in water and air follow the same thermodynamic trajectory and, therefore, require the same action integral h_{water}, this value is smaller by $\Delta h = 0.4\ A^2\,s/cm^4$ than that obtained for UEWE. The fast wire expansion in air starts at $t \approx 1.4\,\mu s$, defining the onset of the wire explosion, t_{exp}, analogous to the UEWE case, where rapid expansion begins at $t \approx 0.9\,\mu s$.

We next assume that at $t_{Imax} \approx 0.94\,\mu s$, when the discharge current reaches its maximum, the entire current still flows through the wire. For later times, the following expression was used for the current flowing through the wire in air,

$$I_w(t) = I(t) \cdot \left[1 + \left(\frac{I'}{I(t_{exp})} - 1\right) \cdot \frac{t - t_{Imax}}{t_{exp} - t_{Imax}}\right], \tag{2}$$

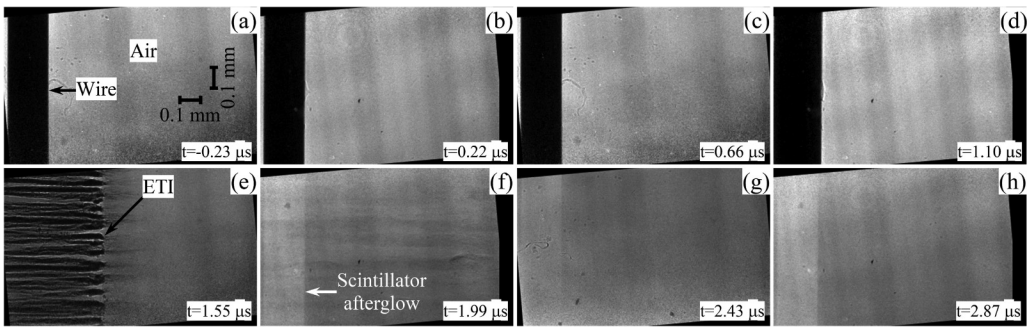

FIG. 6. Same as Fig. 3 but for a 0.20 mm diameter Cu wire explosion in air.

where $I(t)$ is the total measured current, I' is the value of the current through the wire at t_{exp} (see Fig. 7), and $I(t_{exp})$ is the value of the measured total current at t_{exp}. Using this dependence, one can see that at $t = t_{Imax}$, all the current flows through the wire, and at $t = t_{exp}$, the current through the wire is $I_w(t) = I(t) \cdot \frac{I'}{I(t_{exp})}$. Finally, by using $\Delta h = \int_{t_{Imax}}^{t_{exp}} \frac{I_w^2(t)}{S^2(t)} dt$, the value of $I' = 6$ kA was obtained (see Fig. 7).

Let us note that at $t_{exp} \approx 1.4\,\mu$s, the total resistance of the wire–plasma system is $\sim 2\,\Omega$, which indicates that the wire and plasma channel have $\sim 4\,\Omega$ resistance each. The large wire resistance can be attributed to the formation of a weakly ionized, high-resistivity plasma. In fact, it is well known that explosions of long wires in air exhibit pronounced current dwell times, which is consistent with comparable resistances of the wire and the surrounding plasma channel. These estimates, though crude given our assumptions, suggest that at the time of the explosion, only ~52% of the discharge current flows through the wire and contributes to its Ohmic heating.

We consider that the current shunting occurs due to gas ionization near the wire surface. At maximal current, the resistive voltage across the wire's length is ~5.4 kV, which results in a radial electric field component near the HV electrode of $E_r = V_{I_{max}}/(r \ln R/r_0) \sim 84$ kV/cm, where $r_0 = 0.1$ mm is the wire radius and $R = 60$ mm is the radius of the experimental chamber. At $t = 1\,\mu$s, if the current mainly flows through the wire, the deposited energy reaches ~19 J, which exceeds the energy needed to melt the wire at its melting temperature of $T = 1383$ K, but not sufficient to vaporize it completely at $T = 2835$ K (see Fig. 5). The temperature increase causes electron thermionic emission from the wire, described by the Richardson–Dushman equation,[46]

$$J = A\, T^2\, e^{-\phi/k_B T}, \tag{3}$$

where $A = 1.2 \times 10^6$ A m^{-2}K^{-2} is the Richardson constant, $\phi \approx 4.7$ eV is the work function of the metal, and

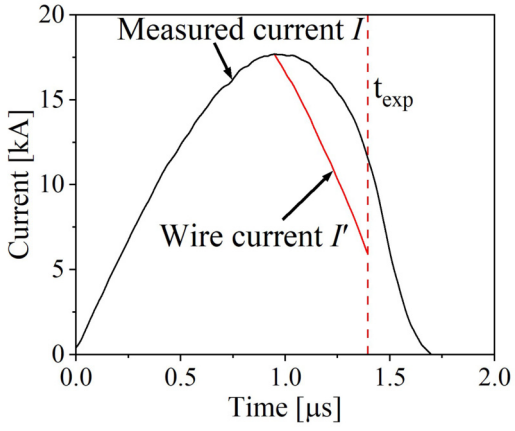

FIG. 7. Estimation of the current flowing through the wire (red) after the moment of maximal current.

$k_B = 1.38 \times 10^{-23}$ m^{2}kg s^{-2}K^{-1} is Boltzmann's constant. Significant electron emission of $>10^3$ electrons/(cm^2 ns) occurs when the temperature reaches 1800 K, and at peak current discharge amplitude when $T \leq 2835$ K, thermionically emitted electron current density reaches $J \leq 4.3$ A/cm^2, corresponding to $>4.5 \times 10^4$ electrons/(cm^2 ns). The average energy which electrons acquire between collisions can be estimated as $\epsilon_e = eE_r\lambda$, where $\lambda = (n_n\sigma_t)^{-1}$ is the mean free path, n_n is the neutral number density, and total cross section of electron collisions is $\sigma_t = \sigma_i + \sigma_s + \sigma_{ex} + \sigma_{dis} \approx 2 \times 10^{-15}$ cm^2,[47] where σ_i, σ_s, σ_{ex}, σ_{dis} are cross section for ionization, total scattering including elastic scattering and momentum transfer, excitations of rotational, vibrational, and electronic states and dissociation, respectively. The neutral density can be estimated considering heating of air in the vicinity of the wire. Using solution of the thermal diffusion equation in one-dimensional approximation, the time/space dependent temperature distribution reads

$$\frac{T(x,\,t) - T_0}{T_s - T_0} = \mathrm{erfc}\left(\frac{x}{2\sqrt{\alpha t}}\right), \tag{4}$$

where $\alpha \approx 5 \times 10^{-5}$ m^2/s is the thermal diffusivity of air, $T_0 \sim 300$ K is the ambient temperature, and $T_s = 2835$ K is the boiling temperature of the Cu wire surface. For a characteristic time of ~300 ns, when the wire temperature reaches $T_s = 2835$ K, the diffusion length is $x = \sqrt{\alpha t} \approx 3.9 \times 10^{-6}$ m, which yields $\mathrm{erfc}(x/(2\sqrt{\alpha t})) \, 0.72$ for $x = 2\,\mu$m. Thus, for $T_s - T_0 \approx 2535$ K, the temperature at $x = 2\,\mu$m and $t = 300$ ns is $T(2\,\mu\text{m}, 300\text{ ns}) \approx 2150$ K. Since the acoustic time $\tau_{ac} = x/c_s < 1$ ns (with sound velocity in hot air of $c_s > 330$ m/s) is much faster than the heating time (~300 ns), the heating process can be considered approximately isobaric. Assuming ideal gas approximation, $p = \mathrm{Const} = \rho RT$, where R is the universal gas constant, the density of the gas ρ decreases by a factor of ~7. This results in mean free path of $\lambda = (n_n\sigma_t)^{-1} \approx 1.34\,\mu$m, meaning electrons acquire an energy of $\epsilon_e = eE_r\lambda \approx 11.3$ eV between collisions for $E_r \sim 84$ kV/cm. This energy is smaller than nitrogen molecules ionization energy of 15.58 eV, but very close to the ionization energy of oxygen molecules which is 12.07 eV.[48] Although these estimates which involve the statistical nature of λ are very crude, they suggest that ionization of the surrounding gas by thermionically emitted electrons is plausible. This process initiates at the HV electrode, and due to the axial electric field and electron avalanching, a plasma channel forms along the entire length of the wire, capturing a significant portion of the discharge current.

B. Analysis of ETI development in Cu wires of different diameters

Electrical parameters of explosions for 0.16 and 0.25 mm diameter Cu wires, along with radiography of ETI development, are shown in Figs. 8–11, respectively. For the 0.16 mm diameter wire, the current waveforms indicate an underdamped explosion characterized by a decaying current oscillation, and the melting and vaporization times based on Fig. 8(b) are ~0.42 and ~0.66 μs. The peak average current density was $\sim 8.7 \times 10^7$ A/cm^2, with energy density and maximum energy density deposition rate at FWHM of

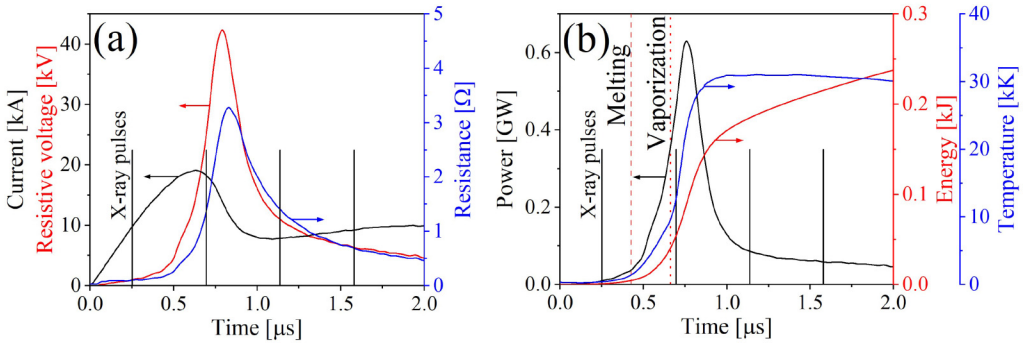

FIG. 8. Same as Figs. 2(a) and 2(b), but for a 0.16 mm diameter Cu wire.

~23.1 kJ/g and $\sim 7.8 \times 10^{10}$ J/(g s), respectively. At $t = 0.7\,\mu$s [Fig. 10(c)], which is the maximum current point, radiography shows that the wire channel radius has already started to expand at an average velocity of ~480 m/s, the onset of the ETI can be seen on the wire edges. At $t = 1.15\,\mu$s [Fig. 10(d)], radiography suggests that the wire has transitioned into low-resistivity plasma, and the ETI appears "smeared" due to expansion and heat conduction. In this case, the ETI occurs after the liquid–vapor phase transition [Fig. 10(c)]. The 0.25 mm diameter wire (Fig. 9) shows a much later explosion process [no observed radial expansion is observed in radiography before $t = 1.14\,\mu$s, see Fig. 11(d)] due to its larger cross section, receiving enough energy for melting only at ~0.68 μs and for vaporization at ~1.38 μs. At FWHM, the energy density and the energy density deposition rate of this wire, with an efficiency of 67%, were 12.6 kJ/g and $\sim 1.4 \times 10^{10}$ J/(g s), respectively, while the average current density was lower, estimated at $\sim 4.9 \times 10^{7}$ A/cm^2. Radiography of the initially 0.25 mm wire shows significant expansion only at $t = 1.58\,\mu$s [Fig. 10(e)], with an average velocity being ~370 m/s. ETI is not observed before this time, meaning prior to the transition into vapor-low ionized plasma phase. To summarize both cases, i.e., 0.16 mm and 0.25 mm diameter wires, the ETI instabilities occurred only after vaporization.

Next, we present a Fourier analysis of the ETI wavelength at high spatial resolution for a 0.20 mm diameter Cu wire (Fig. 12) and for 0.16 mm diameter and 0.25 mm diameter Cu wires [Figs. 13(a) and 13(b), respectively]. One can see that despite the different cross-sectional areas, the measured wavelength remains mostly consistent across tested wires (Fig. 12). Unlike EWE in vacuum and air,[7] we also report that the onset of ETI in wires exploded underwater only becomes observable after vaporization of the material, regardless of their initial cross sections. This may be related to the wire material in an underwater explosion maintaining higher density and heat conductivity, which prevents further development of ETI. Let us note that, in this experiment, the derivative of resistance with respect to temperature is estimated to be positive from the onset of melting and in later times, which is necessary for the development of unstable ETI modes.[26]

The interpretation of the ETI spectra should be approached with caution since the density in the non-uniform wire acts as a spatial comb for the incident x rays. For the current experimental setup (20 keV x-ray energy, $\lambda = 0.062$ nm, and a scintillator located at $z \sim 0.6$ m), the Fresnel scale[49] is $L_F = \sqrt{\lambda z} \approx 6\,\mu$m. This implies that the ~30 μm striation wavelengths are large enough to be resolved in this system. However, striations smaller

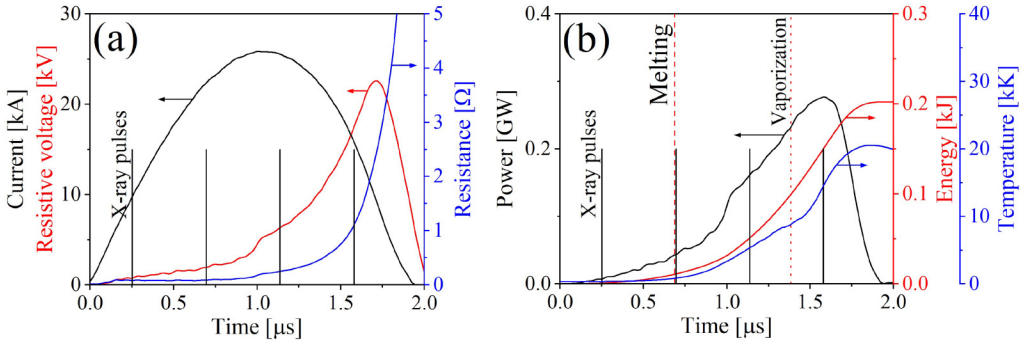

FIG. 9. Same as Figs. 2(a) and 2(b), but for a 0.25 mm diameter Cu wire.

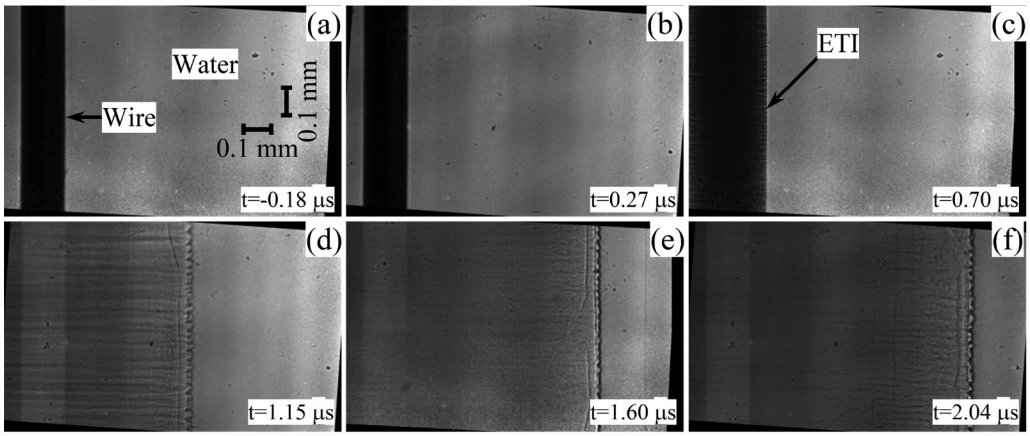

FIG. 10. Same as Fig. 3, but for a 0.16 mm diameter Cu wire explosion in water.

than <12 μm will not be resolved due to their size being comparable to the Fresnel wavelength (grayed-out area in Figs. 12 and 13). Therefore, the Fourier spectra shown in Figs. 12 and 13 are only reliable for wavelength >12 μm. One can observe similar ETI wavelengths for the 0.16 and 0.25 mm wires, as well as a tendency indicating that the wavelength increases over time.

In the next paragraphs, we demonstrate that the linear ETI model[7] ceases to be applicable at later times of UEWE by using the quasi-monochromatic properties of the EuXFEL beam. In Fig. 14(a), we present a close-up image of the 0.20 mm diameter wire at $t = 1142$ ns [Fig. 3(d)], where the ETI was most noticeable. From the background intensity I_0 [blue line in Fig. 14(a)] and the observed ETI intensity I_{obs} at a radius of $r' = 0.3$ mm [red line, Fig. 14(a)], the inferred density of the wire ρ can be calculated using the extinction law,

$$I_{obs} = I_0 e^{-(\mu/\rho)\rho l_{obs}}, \tag{5}$$

where $\mu/\rho \approx 33.8$ cm^2/g is the mass-attenuation coefficient at 20 keV energy[50] and $l_{obs} = 2\sqrt{r^2 - r'^2} \approx 0.36$ mm is the length of the chord traveled by the x rays inside the wire, having a radius of $r = 0.35$ mm at this time and $r' = 0.3$ mm is the length of the apothem. The density of the wire at this location is shown in Fig. 14(c), and the average density of the bright (hot, low-density layer) and dark (cold, compressed layer) strips calculated using this method is estimated as $\rho_{\text{hot}} = 0.3 \pm 0.1$ g/cm^3 and $\rho_{\text{cold}} = 1.9 \pm 0.1$ g/cm^3, respectively. An average density, estimated as $\rho_{\text{avg}} = \rho_0[r_0/r(t)]^2 \approx 0.73$ g/cm^3, is marked with a dashed black line in Fig. 14(c). The corresponding number densities of the hot and cold layers given by $n = \rho N_A/m_W$ are $n_{\text{hot}} \approx 2.8 \times 10^{21}$ cm^{-3} and $n_{\text{cold}} \approx 1.8 \times 10^{22}$ cm^{-3}, with $N_A = 6.022 \times 10^{23}$ mol^{-1} being the Avogadro constant and $M_W = 63.546$ g/mol is the molar mass of copper.[43]

This density may allow one to roughly estimate the validity of the linear ETI approximation in this case, which considers a small deviation of temperature from its average value across the wire's cross section.[7] In a rough approximation, we treat the hot and cold ETI layers as ideal gases with corresponding temperatures $T_{\text{hot}} > T_{\text{cold}}$ and densities $n_{\text{hot}} < n_{\text{cold}}$ that vary from the mean density and temperature $\bar{n}$, $\bar{T}$ by some respective amount

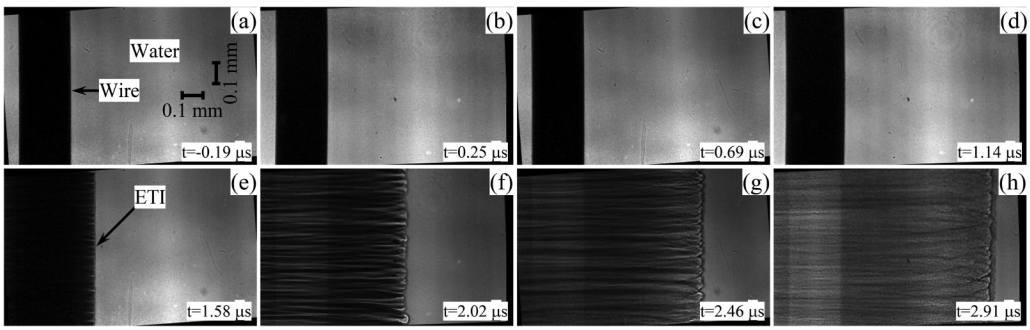

FIG. 11. Same as Fig. 3, but for a 0.25 mm diameter Cu wire explosion in water.

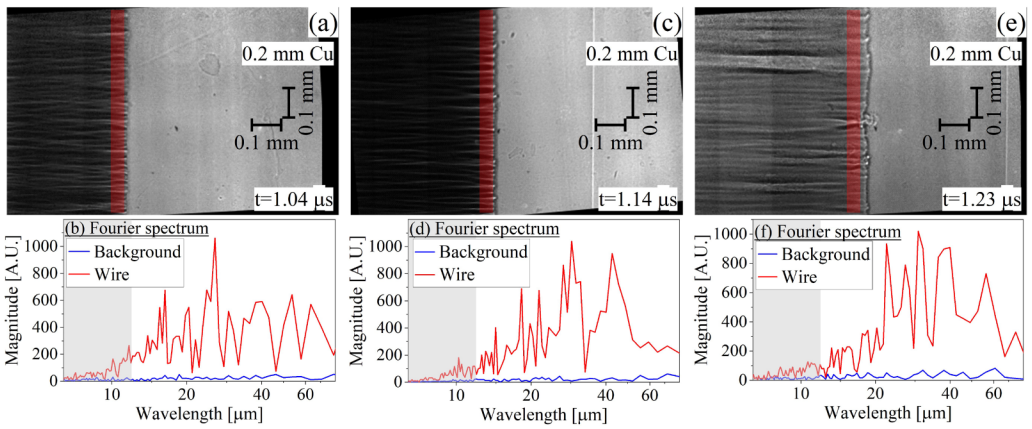

FIG. 12. ETI in x-ray radiography of three different experiments with exploded 0.20-mm diameter Cu wire, highlighted in red [(a), (c), and (e)], and their corresponding Fourier spectrum [(b), (d), and (f)] of before the current onset (noted "Background") and at the explosion (noted "Wire").

Δn, ΔT,

$$T_{\mathrm{hot,cold}} = \bar{T} \pm \Delta T\,, \tag{6}$$

$$n_{\mathrm{hot,cold}} = \bar{n} \mp \Delta n\,. \tag{7}$$

By equating the pressures of the layers using the ideal gas law $n_{\mathrm{hot}} T_{\mathrm{hot}} = n_{\mathrm{cold}} T_{\mathrm{cold}}$ and utilizing the average density values from an x-ray radiography image with a density perturbation of ±50%, we estimate the ratio of layer temperatures to be $T_{\mathrm{cold}}/T_{\mathrm{hot}} \approx 3.3$. Together with Eq. (6), the temperature perturbation scale $\Delta T/\bar{T}$ may be expressed as

$$\frac{\Delta T}{\bar{T}} = \frac{T_{\mathrm{hot}} - T_{\mathrm{cold}}}{T_{\mathrm{hot}} + T_{\mathrm{cold}}}, \tag{8}$$

which is calculated to be $\Delta T/\bar{T} \approx 0.53$ in the present study. Thus, caution is required when applying the linear ETI model at later times during UEWE[26] as significant temperature variations develop following wire vaporization.

Given the large temperature perturbations inferred above, we next estimate the power density deposited in the hot, low-density and cold, high-density layers. Using the average simulated temperature $\bar{T} \approx 28$ kK at $t = 1145$ ns (see Fig. 2), temperatures of ~13.2 and ~42.8 kK are obtained for the cold and hot layers, respectively. Using the data presented in Refs. 10 and 51, we estimate a

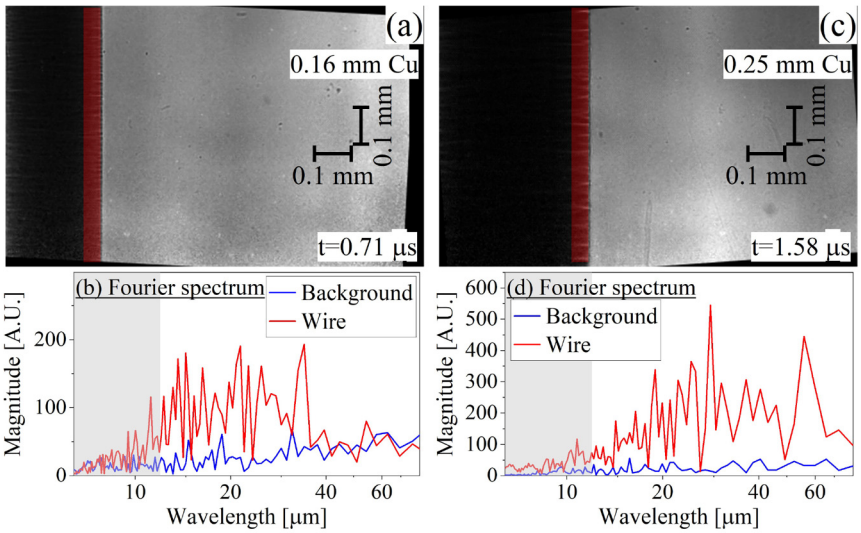

FIG. 13. Same as Fig. 12, but for 0.16 mm Cu wire [(a) and its ETI spectrum in (b)] and 0.25 mm Cu wire [(c) and its ETI spectrum in (d)].

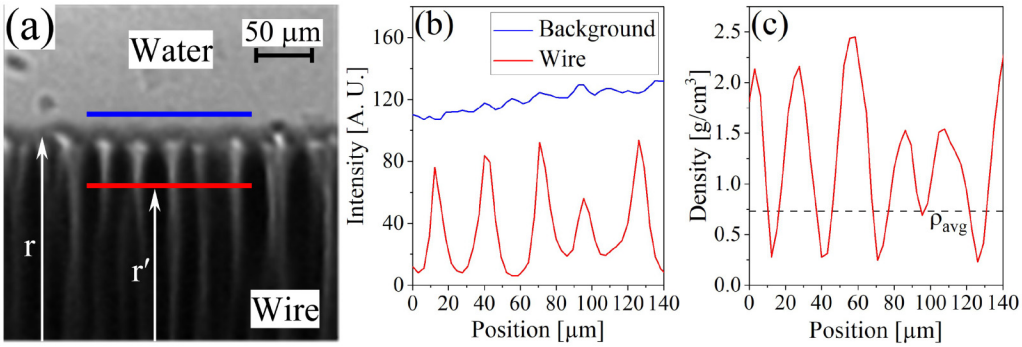

FIG. 14. (a) Section of the wire with lines indicating where the background (blue) and wire (red) intensity profiles were taken. (b) Intensity plot. (c) Density plot calculated based on the extinction law and background intensity.

conductivity $\sigma \approx 1.8 \times 10^5\ \Omega^{-1}\,m^{-1}$ for the high-density layer with $\rho = 1.9\ g/cm^3$ and low temperature (~13.2 kK), whereas for the low-density layer with $\rho = 0.3\ g/cm^3$ and high temperature (~42.8 kK), the conductivity is $\bar{\sigma} < 2 \times 10^4\ \Omega^{-1}\,m^{-1}$. Thus, assuming a uniform current density across the wire cross section, with $j \approx 6.5 \times 10^6$ at $t = 1145$ ns, the deposited power densities are $\sim 2.3 \times 10^{10}$ and $\lesssim 2 \times 10^{11}\ W/cm^3$ for the high- and low-density layers, respectively. At this time, the average conductivity is $\bar{\sigma} \approx 9 \times 10^4\ \Omega^{-1}\,m^{-1}$, as inferred from the measured resistance and wire cross section shown in Figs. 2(a) and 2(c). This value is lower by a factor of two than the conductivity $\bar{\sigma} \approx 2 \times 10^5\ \Omega^{-1}\,m^{-1}$ predicted by the semiempirical model of Stephens *et al.* and by the quantum Lee–More–Desjarlais model for a temperature of 28 kK and an average copper density of $\bar{\rho} = 1.4\ g/cm^3$.[51,52]

C. Instability in UEWE of Cu and Al

Figure 15 presents waveforms for the explosion of a 0.25 mm diameter Al wire in water. The explosion begins at ~1.02 μs, with a similar current amplitude of ~22.5 kA and average current density of $\sim 4.2 \times 10^7\ A/cm^2$, as measured in the Cu wire explosion case (see Fig. 2). At ~1.33 μs, an energy density of ~40.3 kJ/g is delivered into the Al wire at a maximal rate of $\sim 8 \times 10^{10}$ J/(g s) with efficiency of ~66%. The wire's resistance reaches ~2 Ω, similar to the case of Cu wire explosion in water.

X-ray radiography of Al wire explosion demonstrating the development of a large-scale instability is shown in Fig. 16. In this experiment, the two cameras recording the MHz radiography were focused on slightly different areas of the wire. Due to differences in the placement of the instability, the frames in each row of Fig. 16 are arranged according to the respective camera [i.e., Figs. 16(a)–16(f) belong to camera 1 and 2, respectively]. Regardless of which camera recorded the radiography, unlike the uniform front of the expanding wire material seen for Cu in Fig. 3, Al wires exhibit rapid development of large-scale instability, with a difference of up to ~0.15 mm between the wire's smallest and largest radii. The average expansion velocity of the Al wire was similar to that of the Cu wire and was estimated at ~470 m/s from the onset of explosion.

Currently, we cannot determine the origin of this instability. It may be related to inhomogeneities in the aluminum wire itself;

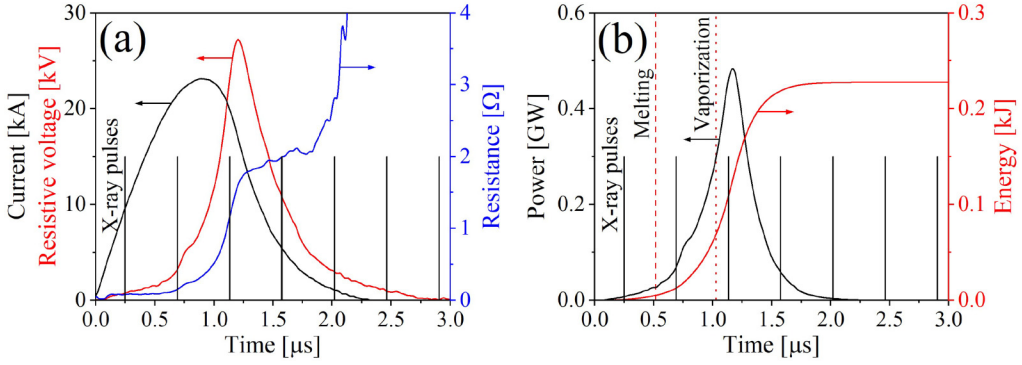

FIG. 15. Same as Figs. 2(a) and 2(b), but for a 0.25 mm diameter Al wire explosion underwater (excluding the simulated temperature).

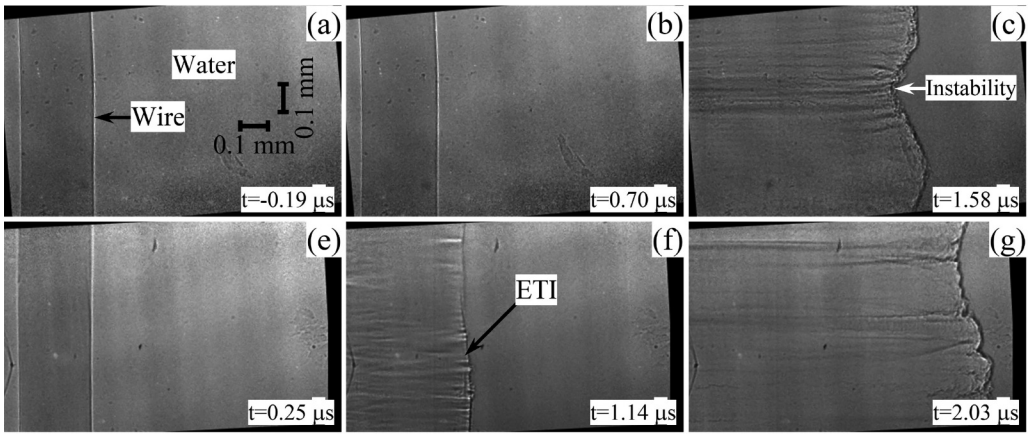

FIG. 16. Same as Fig. 3 but for a 0.25 mm diameter Al wire explosion in water. Frames are grouped by camera to highlight instability development for each camera.

additionally, local aluminum combustion cannot be excluded. In earlier studies,[53,54] sub-microsecond ignition of aluminum combustion was observed during underwater electrical explosions of aluminum wires with diameters of tens of micrometers. Nevertheless, we will discuss the possible development of MHD $m = 0$ or the Rayleigh–Taylor (RT) instability.[55]

First, we consider the typical time for $m = 0$ linear MHD instability development, which can be estimated as the time needed for an Alfven wave to cross the radius of the wire,[7,29]

$$\tau_{m=0} \approx \frac{2}{j}\sqrt{\frac{\rho}{\mu_0}}, \tag{9}$$

where ρ is the material density and μ_0 is the vacuum permeability. It should be noted that the complete melting of Cu wires with diameters of 0.16, 0.20, and 0.25 mm occurs at 0.42, 0.55, and 0.68 μs, respectively, and the 0.25 mm diameter Al wire melts at about 0.52 μs, all relative to the start of the discharge current. From this time, the $m = 0$ instability may begin to develop, and its growth time $\tau_{m=0}$ becomes time dependent due to the increasing wire radius, the corresponding decrease in density, and the time-varying discharge current. Figure 17 shows the calculated time dependence of $\tau_{m=0}$ based on Eq. (9) and on simulated current, radius, and density for 0.16, 0.20, and 0.25 mm diameter Cu wires. For the 0.25 mm diameter Al wire, the experimental current waveform and x-ray radiographic data, which provide information on wire expansion, were used. One can see that for all types of wires, this instability can be developed. However, in experiments, this instability was not observed during Cu wire explosions. Thus, we conclude that the $m = 0$ instability is unlikely to be responsible for the observed phenomenon.

Next, we consider the RT instability, which can be realized only when a heavier fluid accelerates toward a lighter one.[55] However, based on radiography images for Al, at $t = 1.14\,\mu$s, the Al wire density decreases to $\rho_h \sim 0.68$ g/cm^3, which is lower than the density of water. At this time, the wire expansion is already decelerating, as inferred from the concave $r(t)$ trajectory shown in Fig. 2(c) for Cu. Thus, the necessary condition for RT instability at the wire–water interface, $\nabla p \cdot \nabla \rho < 0$ (where ∇p and $\nabla \rho$ are the pressure and density gradients, respectively), is not satisfied. This is reflected in the negative value of the Atwood number, resulting in an imaginary growth rate for this instability. However, the development of RT instability cannot be excluded at earlier times, when the wire density still exceeds that of water (the wire density decreases below 1 g/cm^3 at ~1.09 μs) and the wire expansion occurs under deceleration. At later times, as the wire expansion slows further and its density decreases below that of water, this instability relaxes. Nonetheless, in experiments with Cu wire explosions, this instability development was not observed. This likely relates to the significantly better surface finish of Cu wires compared to Al wires and the less pronounced surface ETI feedback in Cu wires.

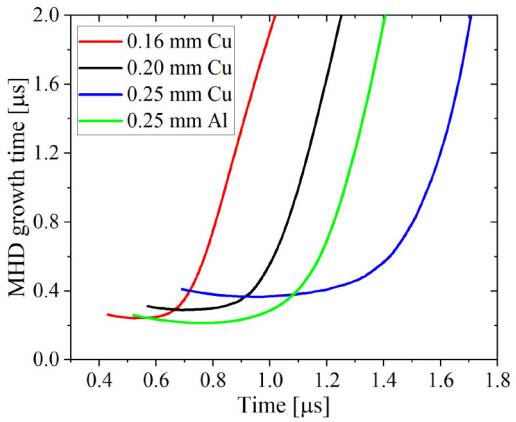

FIG. 17. Temporal dependence of the MHD growth time τ_{inst} for 0.16/0.20/0.25 mm diameter Cu wires (red, black, and blue, respectively) and for 0.25 mm diameter Al wire (green).

IV. SUMMARY

In this study, multi-frame quasi-monochromatic x-ray radiography performed at the EuXFEL was used to investigate several phenomena associated with electrical wire explosions of copper and aluminum in water and in air. First, analysis of shadow images and current waveforms from 0.20 mm copper wires exploded in air allowed, for the first time, a quantitative estimate of the fraction of current shunted through the surrounding medium by comparing them with underwater explosions. In the present microsecond-timescale generator, the shunted current is estimated to be ∼50% of the total measured current at the moment of explosion.

Second, the evolution of the electrothermal instability (ETI) over time was studied in copper wires with diameters of 0.16, 0.20, and 0.25 mm. The results indicate that this instability becomes resolvable after the transition to vapor/plasma phase and the observed explosion. At that time, FFT reveals wavelengths ranging from 20 to 60 μm that do not grow significantly over time and are not strongly dependent on the initial wire diameter.

Additionally, using density measurements of the ETI striation and assuming an ideal gas equation of state, it is shown that the scale of the temperature perturbation in these layers is ∼50% of the wire's average temperature. This makes the application of the linear ETI model for comparison with experimentally obtained ETI challenging when wire transfers to the vapor–plasma state.

Finally, x-ray radiography revealed developing non-uniformity in the Al wire, which is unlikely to be caused by MHD $m = 0$ or Rayleigh–Taylor instability. Instead, we suggest that this behavior may be related to local inhomogeneities in the Al wire or its oxide coating, leading to an earlier explosion at this location. However, confirmation of this mechanism requires further study.

ACKNOWLEDGMENTS

We are grateful to Dr. John Leopold for fruitful discussions. This research was supported by Israel Science Foundation (Grant No. 418/22), EPSRC, and First Light Fusion under the AMPLIFI Prosperity Partnership EP/X025373/1 and the NNSA under No. DOE DE-NA0004148. We acknowledge European XFEL in Schenefeld, Germany, for provision of X-ray free-electron laser beamtime at Scientific Instrument SPB/SFX SASE1 under proposal No. 8012 and would like to thank the staff for their assistance. P. Vagovic and J. Koliyadu acknowledge Thomas Dietze for technical support. P. Vagovic also acknowledges funding from the HORIZON-EIC-2021-PATHFINDEROPEN-01-01 call, as part of the TOMOSCOPY project (Grant Agreement No. 101046448) and EuXFEL R&D "MHz X-ray microscopy: From demonstration to method," 2020–2022. Data recorded for the experiment at the European XFEL are available at doi:10.22003/XFEL.EU-DATA-008012-00.

AUTHOR DECLARATIONS

Conflict of Interest

The authors have no conflicts to disclose.

Author Contributions

R. Grikshtas: Conceptualization (equal); Data curation (equal); Formal analysis (equal); Investigation (equal); Methodology (equal); Resources (equal); Validation (equal); Visualization (equal); Writing – original draft (equal); Writing – review & editing (equal). **N. Asmedianov:** Conceptualization (equal); Data curation (equal); Investigation (equal); Methodology (equal); Resources (equal); Software (equal); Validation (equal); Writing – review & editing (equal). **S. Pavlov:** Software (equal); Visualization (equal). **I. Yungerman:** Software (equal). **A. Rososhek:** Validation (equal); Writing – review & editing (equal). **J. Strucka:** Conceptualization (equal); Formal analysis (equal); Investigation (equal); Methodology (equal); Project administration (equal); Software (equal); Validation (equal); Writing – review & editing (equal). **K. Mughal:** Data curation (equal); Investigation (equal). **B. Lukic:** Data curation (equal); Investigation (equal). **M. Liverts:** Data curation (equal); Investigation (equal). **T. White:** Data curation (equal); Investigation (equal). **R. Bean:** Data curation (equal); Investigation (equal); Methodology (equal); Project administration (equal); Resources (equal). **J. Bielecki:** Data curation (equal); Investigation (equal); Methodology (equal); Software (equal). **R. Letrun:** Data curation (equal); Investigation (equal); Methodology (equal); Software (equal). **T. Popelar:** Data curation (equal); Investigation (equal); Methodology (equal); Software (equal). **E. Sobolev:** Data curation (equal); Investigation (equal); Methodology (equal); Software (equal). **F. Trost:** Data curation (equal); Investigation (equal); Methodology (equal); Software (equal). **J. C. P. Koliyadu:** Data curation (equal); Investigation (equal); Methodology (equal); Resources (equal); Software (equal); Validation (equal); Writing – review & editing (equal). **T. Sato:** Data curation (equal); Investigation (equal); Methodology (equal); Software (equal). **P. Vagovic:** Data curation (equal); Investigation (equal); Methodology (equal); Project administration (equal); Resources (equal); Software (equal); Validation (equal); Writing – review & editing (equal). **S. N. Bland:** Conceptualization (equal); Data curation (equal); Formal analysis (equal); Funding acquisition (equal); Investigation (equal); Methodology (equal); Project administration (equal); Resources (equal); Supervision (equal); Validation (equal); Writing – review & editing (equal). **Ya. E. Krasik:** Conceptualization (equal); Data curation (equal); Formal analysis (equal); Funding acquisition (equal); Investigation (equal); Methodology (equal); Project administration (equal); Resources (equal); Supervision (equal); Validation (equal); Writing – original draft (equal); Writing – review & editing (equal).

DATA AVAILABILITY

Data recorded for the experiment at the European XFEL are available in the European XFEL Scientific Data Repository (EuXFEL myMdC) at https://doi.org/10.22003/XFEL.EU-DATA-008012-00, Ref. 56.

REFERENCES

[1]V. E. Fortov and I. T. Iakubov, *The Physics of Non-Ideal Plasma* (World Scientific, Singapore, 2000).
[2]R. P. Drake, *High-Energy-Density Physics: Fundamentals, Inertial Fusion, and Experimental Astrophysics* (Springer, Berlin, 2006).

[3]*Exploding Wires: Volumes 1–4*, edited by W. G. Chace and H. K. Moore (Plenum Press, New York, 1959).
[4]E. V. Krivitskii, *Dynamics of Electrical Explosion in Liquid* (Naukova Dumka, Kiev, 1983).
[5]A. V. Luchinskii, *Electrical Explosions of Conductors* (Nauka, Moscow, 1989).
[6]V. Burtsev, N. Kalinin, and A. Luchinsky, *Electrical Explosion of Conductors and Its Application in Electrophysical Installations* (Energoatomizdat, Moscow, 1990).
[7]V. I. Oreshkin and R. B. Baksht, IEEE Trans. Plasma Sci. **48**, 1214 (2020).
[8]A. W. DeSilva and J. D. Katsouros, Int. J. Thermophys. **20**, 1267 (1999).
[9]A. E. Barysevich and S. L. Cherkas, Phys. Plasmas **18**, 052703 (2011).
[10]D. Sheftman and Y. E. Krasik, Phys. Plasmas **18**, 092704 (2011).
[11]D. D. Ryutov, M. S. Derzon, and M. K. Matzen, Rev. Mod. Phys. **72**, 167 (2000).
[12]T. A. Shelkovenko, D. B. Sinars, S. A. Pikuz, K. M. Chandler, and D. A. Hammer, Rev. Sci. Instrum. **72**, 667 (2001).
[13]J. Strucka, J. W. D. Halliday, T. Gheorghiu, H. Horton, B. Krawczyk, P. Moloney, S. Parker, G. Rowland, N. Schwartz, S. Stanislaus, S. Theocharous, C. Wilson, Z. Zhao, T. A. Shelkovenko, S. A. Pikuz, and S. N. Bland, Matter Radiat. Extremes **7**, 016901 (2022).
[14]Y. A. Kotov, J. Nanopart. Res. **5**, 539 (2003).
[15]G. V. Ivanenkov, A. R. Mingaleev, S. A. Pikuz, V. M. Romanova, T. A. Shelkovenko, W. Stepniewski, and D. A. Hammer, J. Exp. Theor. Phys. **87**, 663 (1998).
[16]G. S. Sarkisov, B. S. Bauer, and J. S. De Groot, J. Exp. Theor. Phys. Lett. **73**, 69 (2001).
[17]A. G. Rousskikh, V. I. Oreshkin, S. A. Chaikovsky, N. A. Labetskaya, A. V. Shishlov, I. I. Beilis, and R. B. Baksht, Phys. Plasmas **15**, 102706 (2008).
[18]G. V. Ivanenkov, S. Y. Gus'kov, and D. V. Barishpol'tsev, Plasma Phys. Rep. **36**, 67 (2010).
[19]S. I. Tkachenko, D. V. Barishpoltsev, G. V. Ivanenkov, V. M. Romanova, A. E. Ter-Oganesyan, A. R. Mingaleev, T. A. Shelkovenko, and S. A. Pikuz, Phys. Plasmas **14**, 123502 (2007).
[20]S. I. Tkachenko, A. R. Mingaleev, V. M. Romanova, A. E. Ter-Oganes'yan, T. A. Shelkovenko, and S. A. Pikuz, Plasma Phys. Rep. **35**, 734 (2009).
[21]H. D. Edelson and T. Korneff, J. Appl. Phys. **37**, 2166 (1966).
[22]Y. E. Krasik, A. Fedotov, D. Sheftman, S. Efimov, A. Sayapin, V. T. Gurovich, D. Veksler, G. Bazalitski, S. Gleizer, A. Grinenko, and V. I. Oreshkin, Plasma Sources Sci. Technol. **19**, 034020 (2010).
[23]Y. E. Krasik, S. Efimov, D. Sheftman, A. Fedotov-Gefen, O. Antonov, D. Shafer, D. Yanuka, M. Nitishinskiy, M. Kozlov, L. Gilburd, G. Toker, S. Gleizer, E. Zvulun, V. T. Gurovich, D. Varentsov, and M. Rodionova, IEEE Trans. Plasma Sci. **44**, 412 (2016).
[24]L. Li, D. Qian, X. Zou, and X. Wang, IEEE Trans. Plasma Sci. **46**, 3444 (2018).
[25]J. R. Macdonald, Rev. Mod. Phys. **38**, 669 (1966).
[26]V. I. Oreshkin, Tech. Phys. Lett. **35**, 36 (2009).
[27]E. P. Yu, T. J. Awe, K. R. Cochrane, K. J. Peterson, K. C. Yates, T. M. Hutchinson, M. W. Hatch, B. S. Bauer, K. Tomlinson, and D. B. Sinars, Phys. Rev. Lett. **130**, 255101 (2023).
[28]K. J. Peterson, D. B. Sinars, E. P. Yu, M. C. Herrmann, M. E. Cuneo, S. A. Slutz, I. C. Smith, B. W. Atherton, M. D. Knudson, and C. Nakhleh, Phys. Plasmas **19**, 092701 (2012).
[29]K. B. Abramova, N. A. Zlatin, and B. P. Peregud, Sov. J. Exp. Theor. Phys. **69**, 2007 (1975).
[30]A. L. Surkaev, Tech. Phys. **60**, 981 (2015).
[31]A. G. Rousskikh, R. B. Baksht, V. I. Oreshkin, and A. V. Shishlov, AIP Conf. Proc. **2**, 217 (2002).
[32]S. P. Theocharous, S. N. Bland, D. Yanuka, A. Rososhek, M. P. Olbinado, A. Rack, and Y. E. Krasik, Rev. Sci. Instrum. **90**, 013504 (2019).
[33]D. Yanuka, A. Rososhek, S. Theocharous, S. N. Bland, Y. E. Krasik, M. P. Olbinado, and A. Rack, J. Appl. Phys. **124**, 153301 (2018).
[34]D. Yanuka, A. Rososhek, S. Theocharous, S. N. Bland, Y. E. Krasik, M. P. Olbinado, A. Rack, and E. V. Oreshkin, Phys. Plasmas **26**, 050703 (2019).
[35]D. Maler, S. Efimov, M. Liverts, S. Theocharous, J. Strucka, Y. Yao, W. Proud, A. Rack, B. Lukic, S. N. Bland, and Y. E. Krasik, Phys. Plasmas **29**, 063502 (2022).
[36]R. Grikshtas, N. Asmedianov, O. Belozerov, S. Efimov, J. Strucka, Y. Yao, B. Lukic, A. Rack, S. N. Bland, and Y. E. Krasik, Phys. Plasmas **32**, 032705 (2025).
[37]J. C. P. Koliyadu, D. Moško, E. M. Asimakopoulou, V. Bellucci, Š. Birnšteinová, R. Bean, R. Letrun, C. Kim, H. Kirkwood, G. Giovanetti, N. Jardon, J. Szuba, T. Guest, A. Koch, J. Grünert, P. Szeles, P. Villanueva-Perez, F. Reuter, C.-D. Ohl, M. A. Noack, F. Garcia-Moreno, Z. Kuglerová-Valdová, L. Juha, M. Nikl, W. Yashiro, H. Soyama, D. Eakins, A. M. Korsunsky, J. Uličný, A. Meents, H. N. Chapman, A. P. Mancuso, T. Sato, and P. Vagovič, J. Synchrotron Radiat. **32**, 17 (2025).
[38]V. I. Oreshkin, R. B. Baksht, A. Y. Labetsky, A. G. Rousskikh, A. V. Shishlov, P. R. Levashov, K. V. Khishchenko, and I. V. Glazyrin, Tech. Phys. **49**, 843 (2004).
[39]A. Grinenko, Y. E. Krasik, S. Efimov, A. Fedotov, V. T. Gurovich, and V. I. Oreshkin, Phys. Plasmas **13**, 042701 (2006).
[40]S. P. Lyon and J. Johnson, "SESAME: The Los Alamos National Laboratory equation of state database," Report No. LA-UR-92-3407, 1992.
[41]Y. D. Bakulin, V. F. Kuropatenko, and A. V. Luchinskii, Sov. Phys. Tech. Phys. **21**(9), 1144 (1976).
[42]M. K. Almustafa and M. L. Nehdi, Phys. Fluids **35**, 031302 (2023).
[43]Chemical Rubber Company, *CRC Handbook of Chemistry and Physics: A Ready-Reference Book of Chemical and Physical Data*, 84th ed. (CRC Press, Boca Raton, 2003), Vol. 2003/2004.
[44]V. S. Sedoi, G. A. Mesyats, V. I. Oreshkin, V. V. Valevich, and L. I. Chemezova, IEEE Trans. Plasma Sci. **27**, 845 (1999).
[45]V. I. Oreshkin, S. A. Barengol'ts, and S. A. Chaikovsky, Tech. Phys. **52**, 642 (2007).
[46]*Handbook of Ion Sources*, edited by B. Wolf (CRC Press, Boca Raton, FL, 1995).
[47]Y. Itikawa, J. Phys. Chem. Ref. Data **35**, 31 (2006).
[48]L. C. Pitchford, L. L. Alves, K. Bartschat, S. F. Biagi, M. Bordage, I. Bray, C. E. Brion, M. J. Brunger, L. Campbell, A. Chachereau, B. Chaudhury, L. G. Christophorou, E. Carbone, N. A. Dyatko, C. M. Franck, D. V. Fursa, R. K. Gangwar, V. Guerra, P. Haefliger, G. J. M. Hagelaar, A. Hoesl, Y. Itikawa, I. V. Kochetov, R. P. McEachran, W. L. Morgan, A. P. Napartovich, V. Puech, M. Rabie, L. Sharma, R. Srivastava, A. D. Stauffer, J. Tennyson, J. De Urquijo, J. Van Dijk, L. A. Viehland, M. C. Zammit, O. Zatsarinny, and S. Pancheshnyi, Plasma Processes Polym. **14**, 1600098 (2017).
[49]E. Hecht, *Optics*, 5th ed., global ed. (Pearson, Boston, MA, 2017).
[50]J. H. Hubbell and S. M. Seltzer, *Tables of X-Ray Mass Attenuation Coefficients and Mass Energy-Absorption Coefficients 1 keV to 20 MeV for Elements Z=1 to 92 and 48 Additional Substances of Dosimetric Interest* (Radiation Physics Division, PML, NIST, 1995).
[51]J. Stephens, J. Dickens, and A. Neuber, Phys. Rev. E **89**, 053102 (2014).
[52]M. P. Desjarlais, Contrib. Plasma Phys. **41**, 267 (2001).
[53]A. Rososhek, S. Efimov, A. Goldman, S. V. Tewari, and Y. E. Krasik, Phys. Plasmas **26**, 53510 (2019).
[54]A. Rososhek, S. Efimov, A. Virozub, D. Maler, and Y. E. Krasik, Appl. Phys. Lett. **115**, 074101 (2019).
[55]Y. Zhou, Phys. Rep. **720–722**, 1 (2017).
[56]S. N. Bland, "Multi-frame radiography of high-speed hydrodynamic instability growth driven by a kJ pulsed power platform—from the MHz to the GHz," EuXFEL Proposal No. 8012 (2025), available at https://doi.org/10.22003/XFEL.EU-DATA-008012-00.